

The cyclotron line energy in Her X-1: stable after the decay

R. Staubert¹, L. Ducci¹, L. Ji¹, F. Fürst², J. Wilms³, R.E. Rothschild⁴, K. Pottschmidt⁵, M. Brumback⁶, F. Harrison⁷

¹ Institut für Astronomie und Astrophysik, Universität Tübingen, Sand 1, 72076 Tübingen, Germany

² European Space Agency - European Space Astronomy Center (ESA-ESAC), Operations Dpt., Camino Bajo del Castillo, s/n., Urb. Villafraanca del Castillo, 28692 Villanueva de la Canada, Madrid, Spain

³ Dr. Reimis Sternwarte & Erlangen Center for Astroparticle Physics, Univ. Erlangen-Nürnberg, Sternwartstr. 7, 96049 Bamberg, Germany

⁴ Center for Astrophysics and Space Sciences, University of California at San Diego, La Jolla, CA 92093-0424, USA

⁵ NASA-Goddard Spaceflight Center, 8800 Greenbelt Rd., Greenbelt, MD 20771, USA, Department of Physics and Center for Space Science and Technology, University of Maryland Baltimore County, Baltimore, MD 21250, USA

⁶ Dartmouth College, Department of Physics & Astronomy, 6127 Wilder Laboratory, Hannover, NH 03755, USA

⁷ Cahill Center for Astronomy and Astrophysics, California Institute of Technology, Pasadena, CA 91125, USA

submitted: 06/07/2020, accepted: 17/08/2020

ABSTRACT

We summarize the results of a dedicated effort between 2012 and 2019 to follow the evolution of the cyclotron line in Her X-1 through repeated *NuSTAR* observations. The previously observed nearly 20-year long decay of the cyclotron line energy has ended around 2012: from there onward the pulse phase averaged flux corrected cyclotron line energy has remained stable and constant at an average value of $E_{\text{cyc}} = (37.44 \pm 0.07)$ keV (normalized to a flux level of 6.8 *RXTE*/ASM-cts/s). The flux dependence of E_{cyc} discovered in 2007 is now measured with high precision, giving a slope of (0.675 ± 0.075) keV/(ASM-cts/s), corresponding to an increase of 6.5% of E_{cyc} for an increase in flux by a factor of two. We also find that all line parameters as well as the continuum parameters show a correlation with X-ray flux. While a correlation between E_{cyc} and X-ray flux (both positive and negative) is now known for several accreting binaries with various suggestions for the underlying physics, the phenomenon of a long-term decay has so far only been seen in Her X-1 and Vela X-1, with far less convincing explanations.

Key words. magnetic fields, neutron stars, – radiation mechanisms, cyclotron scattering features – accretion, accretion columns – binaries: eclipsing – stars: Her X-1 – X-rays: general – X-rays: stars

1. Introduction

The eclipsing binary Her X-1/HZ Her is a low mass X-ray binary (LMXB), discovered as an X-ray source by the first X-ray satellite *UHURU* in 1971 (Tananbaum et al. 1972). Similar to Cen X-3, the source was identified as an X-ray pulsar, powered by mass accretion from its companion. Her X-1 is one of the most interesting X-ray pulsars due to its wide variety of observable features. Of the many introductions to this source we refer to some of the most recent ones, e.g., Staubert et al. (2017, 2019); Sazonov et al. (2020). In order to maintain some degree of completeness within this contribution we list the following main features of Her X-1: the spin period of the neutron star is 1.24 s, the orbital period is 1.7 d (identified by eclipses and the modulation of the pulse arrival times), there is a super-orbital flux modulation with a somewhat variable period of ~ 35 d. This *On-Off* variation can be understood as being due to the precession of a warped accretion disk (Pettersen 1977; Schandl & Meyer 1994). Due to the high inclination of the binary ($i > 80^\circ$) we see the disk nearly edge-on (Gerend & Boynton 1976). The precessing warped disk covers the central X-ray source during a substantial portion of the 35 d period (Klochkov et al. 2006, 2008).

The X-ray spectrum Her X-1 is a power law continuum with exponential cutoff, as typical of accreting binary pulsars (Wolff et al. 2016). The cyclotron line around 37 keV, discovered in a balloon observation in 1975 (Trümper et al. 1978), is due to res-

onant scattering of photons by electrons on Landau levels in the $\sim 10^{12}$ Gauss magnetic field at the polar caps of the neutron star. It is therefore often referred to as a cyclotron resonant scattering feature (CRSF). The energy spacing between the Landau levels is approximately given by $E_{\text{cyc}} \approx 11.6 \text{ keV } B_{12}$, where B_{12} is the magnetic field strength in units of 10^{12} Gauss. If the gravitational redshift is taken into account, the magnetic field strength at the site of the emission of the X-ray spectrum can be measured directly from the observed energy of the fundamental cyclotron line in the X-ray spectrum: $B_{12} \approx (1+z) E_{\text{obs}}/11.6 \text{ keV}$, where z is the gravitation redshift (Schwarm et al. 2017).

The discovery of the cyclotron feature in the spectrum of Her X-1 was the first direct measurement of the surface magnetic field strength of a neutron star. Contrary to other ways to estimate such a magnetic field strength, no further model assumptions are needed. We now know about 35 binary X-ray pulsars that show cyclotron lines in their spectra, generally between a few keV and ~ 100 keV (for reviews, see Staubert et al. 2019; Revnivtsev & Mereghetti 2016; Caballero & Wilms 2012; Wilms 2012; Terada et al. 2007; Heindl et al. 2004; Staubert 2003; Coburn et al. 2002).

Significant variability has been observed with the CRSF in Her X-1, regarding its centroid energy E_{cyc} and other characteristic parameters like its width and its optical depth. These parameters do vary with pulse phase, with luminosity, and with time (Staubert et al. 2014). Her X-1 was in fact the source in which all these variations were observed for the first time: a

Send offprint requests to: staubert@astro.uni-tuebingen.de

Table 1. Details on *NuSTAR* observations of Her X-1 between 2012 and 2020.

Observation date	Obs ID	35-day cycle no. ^a	Start of obs [MJD]	End of obs [MJD]	Center of obs [MJD]	Net exposure [ksec]	35-day Turn-On ^b [MJD]	35-day phase ^c of center of obs
22 Sep 2012	30002006005 ^d	427	56192.19	56192.77	56192.48	~22	56189.0 ± 0.1	0.100
03 Aug 2015	90102002002	457	57237.69	57238.26	57237.98	22.5	57233.5 ± 0.1	0.128
20 Aug 2016	10202002002	468	57620.19	57621.26	57620.73	36.6	57617.2 ± 0.1	0.101
05 Aug 2017	30302012002	478	57970.42	57971.21	57970.81	28.4	57965.7 ± 0.2	0.147
26 Feb 2018	30302012004	484	58175.07	58175.79	58175.43	18.3	58171.5 ± 0.5	0.113
17 Sep 2018	30402009002	490	58378.83	58379.56	58379.19	28.4	58377.7 ± 0.3	0.044
09 Feb 2019	30402034002	494	58523.41	58523.85	58523.63	18.3	58516.6 ± 0.2	0.202 ^e
14 Mar 2019	30402034008	495	58556.28	58556.75	58556.51	4.3	58551.5 ± 0.7	0.144
23 Jun 2019	30402009004	498	58657.34	58658.06	58657.70	27.1	58654.1 ± 0.2	0.102

^a 35-day cycle numbering is according to Staubert et al. (1983); ^b as determined from the monitoring data of *Swift*/BAT; ^c using $P_{35} = 34.85$ d; ^d see Fürst et al. (2013), Table 1; ^e this observation is at a particular high 35-day phase.

Table 2. Summary of the spectral analysis of nine *NuSTAR* observations of Her X-1. The spectral parameters were found by applying the XSPEC-function `highecut` (see text). Uncertainties are at the 1 sigma (68%) level. The maximum flux of the respective 35-day cycle is given in units of (ASM-cts/s), referring to the All Sky Monitor of *RXTE*. The corresponding physical flux in units of (keV/cm² s) results by multiplying with 0.2367. The flux was actually measured by *Swift*/BAT and converted according to (2–10 keV) (ASM – cts/s) = 93.0 × (15–50 keV) (BAT – cts/cm² s) (Staubert et al. 2016). The observed line energy was normalized to an ASM-count rate of 6.8 cts/s by using a slope of (0.675 ± 0.075) keV/(ASM-cts/s) (see Fig. 1).

35 d cycle no. ^e	max. flux of 35 d cycle [ASM-cts/s]	Observed line energy [keV]	Line width σ [keV]	Line strength ^a [keV]	E_{cyc} norm. to 6.8 ASM-cts/s [keV]	E_{cut} [keV]	E_{fold} [keV]	Power law index Γ
427	6.60 ± 0.37	37.40 ± 0.25 ^b	5.76 ± 0.29	8.86 ± 0.87	37.54 ± 0.25	20.68 ± 0.27	9.95 ± 0.13	0.920 ± 0.004
457	2.96 ± 0.20	34.79 ± 0.22	4.46 ± 0.22	4.70 ± 0.70	37.38 ± 0.24 ^c	19.86 ± 0.12	9.37 ± 0.09	0.929 ± 0.003
468	6.50 ± 0.20	37.18 ± 0.14	5.97 ± 0.18	8.83 ± 0.44	37.38 ± 0.14 ^c	20.86 ± 0.15	10.16 ± 0.07	0.985 ± 0.001
478	4.10 ± 0.20	35.62 ± 0.18	4.94 ± 0.20	5.90 ± 0.40	37.44 ± 0.19	19.98 ± 0.16	9.79 ± 0.09	0.962 ± 0.002
484	4.09 ± 0.19	35.67 ± 0.29	4.84 ± 0.33	6.10 ± 0.70	37.50 ± 0.30	20.04 ± 0.11	10.16 ± 0.07	0.963 ± 0.002
490	5.60 ± 0.46	36.65 ± 0.16	5.61 ± 0.25	8.44 ± 0.59	37.46 ± 0.16	20.45 ± 0.23	9.79 ± 0.09	0.974 ± 0.002
494	5.02 ± 0.46	36.28 ± 0.22	5.26 ± 0.24	7.21 ± 0.53	37.48 ± 0.23	19.56 ± 0.12	9.65 ± 0.11	0.885 ± 0.002 ^f
495	3.72 ± 0.56	35.36 ± 0.41	4.76 ± 0.45	6.38 ± 0.98	37.44 ± 0.43	19.62 ± 0.29	9.49 ± 0.24	0.934 ± 0.005
498 ^d	4.00 ± 0.37	35.65 ± 0.21	5.01 ± 0.25	7.02 ± 0.50	37.54 ± 0.22	19.81 ± 0.16	9.38 ± 0.09	0.932 ± 0.001

^a we note that strength = $\sigma \tau \sqrt{2\pi}$;

^b the values for the CRSF are from Fürst et al. (2013), Obs. II (Table 3, HighE);

^c in Staubert et al. (2016, 2017) the flux normalization was done with a slope of 0.44 (instead of 0.675);

^d for the June 2019 observation only data from detector B have been used (see text);

^e 35-day cycle numbering is according to Staubert et al. (1983);

^f observation at a high 35-day phase, Γ expected to be lower (Vasco 2012).

positive correlation between E_{cyc} and the X-ray luminosity L_x (Staubert et al. 2007) (confirmed on short timescales by the pulse-amplitude-resolved technique by Klochkov et al. 2011), and a long-term decay of E_{cyc} , co-existing with the luminosity dependence (Staubert et al. 2014, 2016). The long-term decay was confirmed by Klochkov et al. (2015) using monitoring data of *Swift*/BAT¹. For the current knowledge about such variations in other accreting X-ray pulsars see Staubert et al. (2019).

Of particular interest has been the long-term decay and the question whether this would end at some time - or even invert, such that E_{cyc} would rise again. This seemed to have been observed in 2017 (Staubert et al. 2017). We do, however, show here that the decay had ended, but a turn-up did not actually materi-

alize (see Sect. 3.1). The end of the decay is supported through observations with *Swift*/BAT (Ji et al. 2019) and *Astrosat* (Bala et al. 2020).

Here we summarize the results of nine observations of Her X-1 by *NuSTAR*² in the time frame 2012 to 2019 with regard to the cyclotron resonance scattering feature in the pulse averaged X-ray spectrum: the CRSF energy has apparently stopped its ~20-year long decay and has stayed constant since around 2012. In addition to the CRSF centroid energy also its width and strength are clearly correlated with flux, the dependencies are now measured with high precision. We further present evidence for a dependence of all continuum parameters on X-ray flux.

¹ BAT refers to the Burst Alert Telescope on the NASA mission *Swift*

² *NuSTAR* refers to the NASA mission Nuclear Spectroscopic Telescope Array

2. Observations and analysis

In Table 1 we list nine observations of Her X-1 performed by *NuSTAR* (Harrison et al. 2013) over the time period 2012 to 2019, all done close to the maximum flux of a *Main-On* state. Also given are the net exposure times (varying between 4.3 ks and 36.6 ks), the times of the respective 35-day *Turn-On* and the 35-day phase of the center of the respective observations. The details of the data analysis are similar to those described by Staubert et al. (2014) and Staubert et al. (2016). We used the standard *nupipeline* and *nuproducts* utilities (01 Apr 20_v1.9.2) and *XSPEC*³ v12.11 as part of *HEASOFT*⁴. The source extraction diameter was selected between 90 arcsec and 120 arcsec depending on the brightness of the source. All values given are from simultaneous spectral fitting of the data from both focal plane detectors, unless otherwise stated. The spectral function used for all observations was the *XSPEC*-function *highcut* in combination with a power law:

$$I_E = \begin{cases} K \cdot E^{-\Gamma}, & \text{if } E \leq E_{\text{cut}} \\ K \cdot E^{-\Gamma} \exp\left(-\frac{E-E_{\text{cut}}}{E_{\text{fold}}}\right), & \text{if } E > E_{\text{cut}}. \end{cases} \quad (1)$$

where Γ is the power law (photon) index, E_{cut} is the energy where the cut-off sets in, and E_{fold} is the e-folding energy describing the flux decay. The function contains a discontinuity of its first derivative (a “break”) at $E = E_{\text{cut}}$. In order to smooth this break, generally an artificial small Gaussian absorption line was added with the center energy fixed to E_{cut} and a free width and depth. Neither the power law, nor the exponential cut off are affected by this (e.g., Coburn et al. 2002).

The cyclotron line is modeled by the Gaussian shaped “gabs” function: To model the cyclotron line, one modifies the continuum functions described above by the inclusion of a corresponding multiplicative component of the form $e^{-\tau(E)}$, where the optical depth $\tau(E)$ has a Gaussian profile:

$$\tau(E) = \tau_0 \exp\left[-\frac{(E - E_{\text{cyc}})^2}{2\sigma_{\text{cyc}}^2}\right], \quad (2)$$

with τ_0 , E_{cyc} , and σ_{cyc} being the central optical depth, the centroid energy, and the width of the line. We note that in the popular *XSPEC* realization of this function *gabs*, τ_0 is not explicitly used as a fit parameter. Instead, a product $\tau_0 \sqrt{2\pi}\sigma_{\text{cyc}}$ is defined as the “strength” of the line.

Some of the listed *NuSTAR* observations have been performed in coordination with other satellites, like *INTEGRAL*, *Insight-HXMT* and *Astrosat*⁵ to study the CRSF. The February and March 2019 observations were coordinated with *XMM-Newton*⁶ for a different project⁷, but also gave data on the CRSF. Here we will not report on the results from the other satellites because we are still working on trying to resolve some inconsistencies, which are likely due to imperfect inter-calibration between the different instruments and possibly aging of some of them⁸ - we plan to report about this in a forthcoming paper. For first results from *Insight-HXMT* and *Astrosat* see Xiao et al. (2019) and Bala et al. (2020).

³ <https://heasarc.gsfc.nasa.gov/xanadu/xspec/>

⁴ <http://heasarc.nasa.gov/lheasoft>, 6.27.2, caldb release 20191219.

⁵ *INTEGRAL* is the International Gamma-ray Astrophysics Laboratory of ESA, *Insight-HXMT* the Chinese mission Hard X-ray Modulation Telescope, and *Astrosat* the X-ray satellite mission of India

⁶ *XMM-Newton* is ESA's Multi Mirror soft X-ray mission

⁷ Brumback et al. 2020, submitted

⁸ We are still attempting to perform further simultaneous observations between *NuSTAR*, *INTEGRAL* and *Insight-HXMT*, some are already planned.

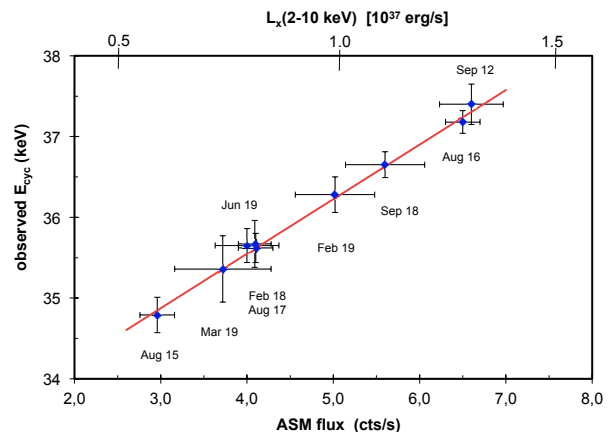


Fig. 1. Correlation between the measured values of the pulse phase averaged cyclotron line energy and the X-ray flux (at the maximum of the respective 35d *Main-On*), as measured by *Swift*/BAT (in units of (ASM-cts/s)) for all *NuSTAR* observations between 2012 and March 2019 (see Table 1). We note that 1 (ASM-cts/s) equals 93.0 (Swift-BAT-cts)/(cm² s) (Staubert et al. 2016) and 0.224 (keV/cm² s) in (2–10 keV). The best fit line defines a slope of (0.675 ± 0.075) keV/(ASM – cts/s). Pearson’s linear correlation coefficient is 0.98. For the mean power law index of -0.953 and an adopted distance of 6.6 kpc (Reynolds et al. 1997), the Her X-1 luminosity is $L_x(2-10 \text{ keV}) [10^{37} \text{ erg/s}] = 0.187(1) \times (\text{ASM-cts/s})$

3. Results

In Table 2 we summarize the results of the spectral analysis, both for the cyclotron line (the centroid energy, the width and the strength) and for the continuum (cut-off energy E_{cut} , e-folding energy E_{fold} and power law index Γ). We further list the maximum fluxes of the respective 35-day cycles.

In order to allow us to do a comparison to previous results, we use the observational flux units of (ASM-cts/s), referring to the All Sky Monitor of *RXTE*⁹, using the conversion (2–10 keV) (ASM-cts/s) = 93.0 × (15–50 keV) (BAT-cts/cm² s). This was found by Staubert et al. (2016) by comparing flux values measured by the All Sky Monitor onboard of *RXTE* on the one hand and those from *Swift*/BAT on the other, for the overlapping time of both missions.

The relationship between ASM (or BAT) count rates and *NuSTAR* and corresponding physical flux units was established in the following way: the observed maximum ASM count rate (from the monitoring observations by *Swift*/BAT) for each 35d cycle (Table 2) was plotted against the normalization, the flux at 1 keV, as determined through the spectral analysis of the corresponding *NuSTAR* observation (cycle 494/Feb 2019 was excluded, since this observation was at a 35d-phase of 0.202, after the maximum flux). This establishes the relationship: flux at 1 keV [photons/cm² s keV] = 0.0255 × (ASM-cts/s), or flux at 1 keV [photons/cm² s keV] = 3.371 × (BAT-cts/cm² s). The energy flux was found by integrating the spectrum over the interested energy range. The following relationships in physical units emerge (taking the mean power law index of -0.953): (2-10 keV flux) [keV/cm² s] = 0.224 × (ASM-cts/s), or (2-10 keV flux) [erg/cm² s] = 3.58 10⁻¹⁰ × (ASM-

⁹ *RXTE* refers to the NASA mission Rossi X-ray Timing Explorer, and ASM to the All Sky Monitor on this satellite

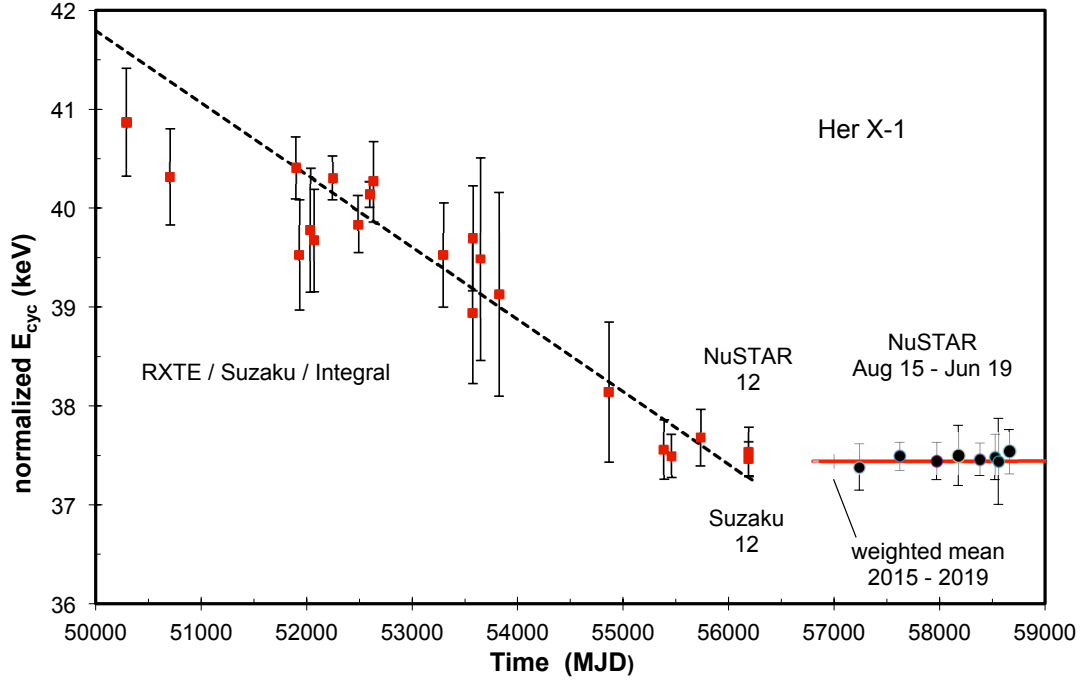


Fig. 2. Evolution of the cyclotron line energy E_{cyc} in Her X-1. The red points until 2012 (MJD 56200) and the corresponding linear best fit (dashed line) are reproduced from Staubert et al. (2016). The black points are the new measurements by *NuSTAR* from 2015-2019 (see Table 1); the pulse phase averaged E_{cyc} values normalized to a reference ASM count rate of 6.8 (ASM – cts/s) using a flux dependence of 0.675 keV/(ASM – cts/s) (see Fig. 1). The solid red line represents the weighted mean of (37.44 ± 0.07) keV, demonstrating a constant value since at least 2012.

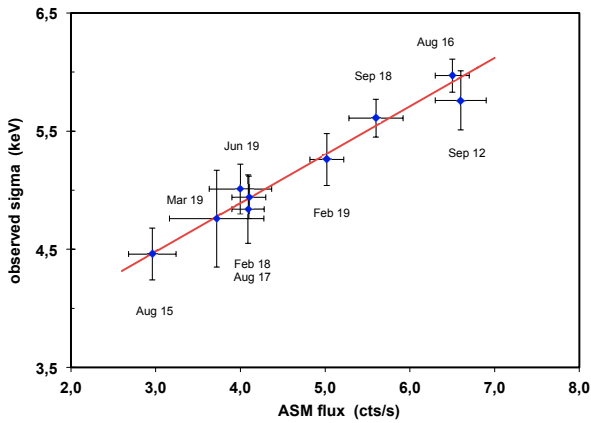


Fig. 3. Correlation between the measured values of the width (sigma) of the cyclotron line and the X-ray flux. The fit takes into account nine measurements by *NuSTAR* from 2012-2019 (see Table 1). The best fit line is given by the function $\text{sig}_{\text{cyc}} = (5.30 \pm 0.09) + (0.41 \pm 0.07) \times ((\text{ASM} - \text{cts/s}) - 5.0)$ (all values in keV). Pearson's linear correlation coefficient is 0.99.

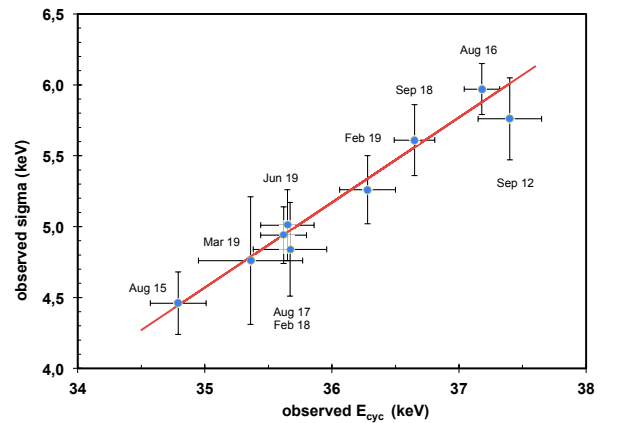


Fig. 4. Correlation between the width (sigma) of the pulse phase averaged cyclotron line and its centroid energy. The fit takes into account nine measurements by *NuSTAR* from 2012-2019 (see Table 1). The best fit line is given by the function $\sigma_{\text{cyc}} = (5.17 \pm 0.09) + (0.60 \pm 0.11) \times (E_{\text{cyc}} - 36.0)$ (all values in keV). Pearson's linear correlation coefficient is 0.96.

cts/s). With a distance of 6.6 kpc to Her X-1 (Reynolds et al. 1997), the corresponding (2-10 keV) luminosities are given by $L_x(2-10 \text{ keV}) [10^{37} \text{ erg/s}] = 0.187(1) \times (\text{ASM-cts/s})$, or $L_x(2-10 \text{ keV}) [10^{37} \text{ erg/s}] = 17.4(1) \times (\text{BAT-cts/cm}^2 \text{ s})$. Also listed

in Table 2 are the cyclotron line energies normalized to a flux of 6.8 (ASM-cts/s) using the determined linear flux dependence (Fig. 1): $E_{\text{cyc-norm}} [\text{keV}] = E_{\text{cyc-obs}} [\text{keV}] + 0.675 \times ((\text{ASM-cts/s}) - 6.8)$. This relation is extremely well established (with a

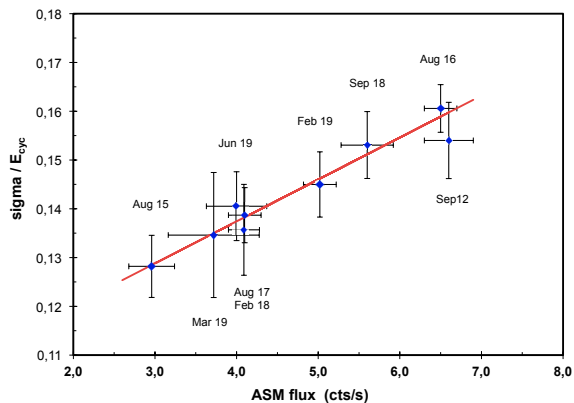


Fig. 5. The relative width of the cyclotron line versus X-ray flux in units of (ASM-cts/s). The best fit line is given by the function $\sigma_{\text{cyc}} / E_{\text{cyc}} = (0.146 \pm 0.002) + (0.0086 \pm 0.0019) \times ((\text{ASM} - \text{cts/s}) - 5.0)$. Pearson's linear correlation coefficient is 0.97.

Pearson's linear correlation coefficient of 0.98¹⁰). The choice of 6.8 (ASM-cts/s) as reference flux is historical and allows a direct comparison to previous results (for all other spectral parameters we now use a reference flux of 5.0 (ASM-cts/s) because this flux is closer to the center of the flux range observed, and nearly corresponds to a (2-10 keV) luminosity of $\sim 10^{37}$ erg/s).

Generally, all parameter values stated are from the combined spectral analysis of both focal plane detectors of *NuSTAR*, except for the observation in June 2019 (cycle 498): only focal plane detector B was used, for E_{cut} the value from detector A is exceptionally high and far outside the overall trend (Fig. 7) (the anomaly is being investigated).

3.1. Cyclotron line parameters

The new data allow us to determine the correlation between the observed pulse averaged cyclotron line energy and the X-ray flux with a significantly improved accuracy when compared to the time of the discovery of this correlation (Staubert et al. 2007). Fig. 1 shows the definite correlation which can be described by the linear function $E_{\text{cyc}} [\text{keV}] = a + b \times ((\text{ASM} - \text{cts/s}) - 6.8)$, with $a = (37.44 \pm 0.07)$ being the CRSF value at an ASM count rate of 6.8 cts/s and $b = (0.675 \pm 0.075)$ keV/(ASM - cts/s) the slope describing the flux dependence.

Figure 2 displays the evolution of the normalized CRSF centroid energy of Her X-1 from 2009 to 2019. The red data points are historical results that were published before, together with the dashed line representing the end of the phase of the long-term decay of E_{cyc} between 1996 and 2012 as reported by Staubert et al. (2016) (their Fig. 2). The right hand side shows the latest values from *NuSTAR* (2015-2019). All data points are flux corrected (normalized to an ASM count rate of 6.8 cts/s). The values since 2015 are apparently consistent with a constant value, the formal weighted average is $\langle E_{\text{cyc}} \rangle (2015 - 2019) = (37.44 \pm 0.07)$ keV. Because there is no time dependence of the normalized E_{cyc} in 2015–2019, it is not necessary to perform a combined fit with simultaneously existing flux and time dependencies,

¹⁰ see, e.g., Numerical Recipes, W.H. Press et al., Cambridge University Press, 1986

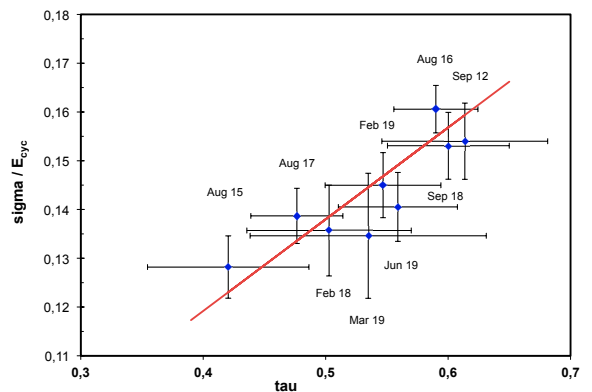


Fig. 6. The relative width of the cyclotron line versus optical depth τ . The best fit line is given by the function $\sigma_{\text{cyc}} / E_{\text{cyc}} = (1.38 \pm 0.005) + (0.188 \pm 0.076) \times (\tau_{\text{cyc}} - 0.5)$. Pearson's linear correlation coefficient is 0.88.

as was done for the data earlier than 2012 (Staubert et al. 2016).

We need to point out, however, that the new data require a modification of the view presented in Staubert et al. (2017), in which it was suggested that an inversion (an upward trend) in E_{cyc} had occurred after the end of the decay. This impression was mainly driven by the 2015 measurement which happened at an extremely low flux level - in fact the lowest of all *NuSTAR* observations at around 3 (ASM-cts/s) (see Fig. 1). This had, on the one hand, turned out to be useful in extending the dynamic range in observed fluxes beyond the (classical) factor of two, it led, on the other hand, to a very low value of the flux normalized E_{cyc} when the correction was done with the then best value of the flux dependence of 0.44 keV/(ASM - cts/s) (Staubert et al. 2016, 2017). When the current best value (0.675 instead of 0.44) is used for the normalization, the 2015 value is significantly higher and consistent with values found throughout 2012–2019 (see Table 1 and Fig. 2).

A further result of our analysis of the nine *NuSTAR* observations is that we find that also all other characteristic parameters of the cyclotron line - the width σ , the "strength", the optical depth τ and the relative width - are linearly correlated with the X-ray flux. In Table 4 we summarize the results of linear fits of all the CRSF line parameters versus flux. This also means that all line parameters correlate with one-another linearly. As an example, Fig. 3 shows the dependence of the line width σ on flux and Fig. 4 the dependence of σ on E_{cyc} . This correlation is a well known behavior (apparently valid for all cyclotron line sources, e.g., Makishima et al. (1999); Coburn et al. (2002)), that is expected to occur through thermal Doppler broadening because of the free movement of electrons along the magnetic field lines (see discussion below). Even though the correlations between the different parameters can in principle be re-constructed from the respective dependencies of all parameters on flux (Table 4), we have performed the linear fits for every possible pair of parameters explicitly and summarize the results in Table 3.

It is worth to note that the relative line width, σ / E_{cyc} , is not constant, but increases with increasing flux (Fig. 5) according to $\sigma / E_{\text{cyc}} = 0.146 + 0.0087 (\text{ASM} - 5.0)$. This means that the relative change with changing flux is stronger for the line width than for the line energy.

Table 3. Relations between line parameters, $y = a + b(x - c)$: parameter y (top line) versus parameter x (first column). The offset c is constant for any given parameter x . Uncertainties are at the 1 sigma (68%) level.

Parameter versus	E_{cyc} [keV]	σ_{cyc} [keV]	strength [keV]	τ	$\sigma_{\text{cyc}} / E_{\text{cyc}}$
E_{cyc}	—	$a = 5.17 \pm 0.09$ $b = 0.60 \pm 0.11$ $c = 36.0 \text{ keV}$	$a = 6.91 \pm 0.22$ $b = 1.71 \pm 0.29$ $c = 36.0 \text{ keV}$	$a = 0.53 \pm 0.02$ $b = 0.064 \pm 0.023$ $c = 36.0 \text{ keV}$	
σ_{cyc}		—	$a = 6.42 \pm 0.31$ $b = 2.84 \pm 0.63$ $c = 5.0 \text{ keV}$	$a = 0.51 \pm 0.02$ $b = 0.11 \pm 0.04$ $c = 5.0 \text{ keV}$	
strength			—	$a = 0.53 \pm 0.02$ $b = 0.041 \pm 0.014$ $c = 7.0$	
τ				—	$a = 0.14 \pm 0.05$ $b = 0.19 \pm 0.08$ $c = 0.50$
E_{cut}		$a = 35.86 \pm 0.11$ $b = 1.87 \pm 0.36$ $c = 20.0 \text{ keV}$			
E_{fold}		$a = 36.69 \pm 0.13$ $b = 2.71 \pm 0.39$ $c = 10.0 \text{ keV}$			

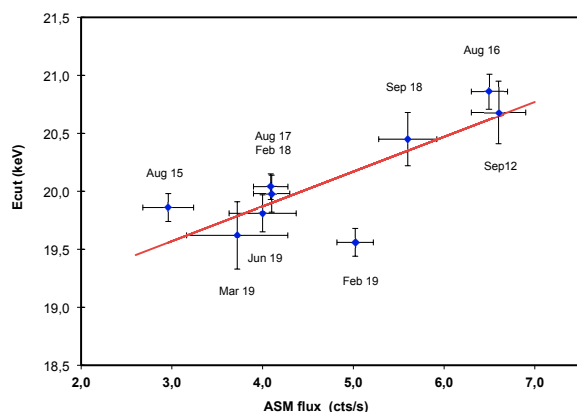


Fig. 7. The continuum parameter E_{cut} versus X-ray flux in units of (ASM-cts/s). The value for the June 2019 observation is from focal plane detector B only (see text). The best fit line is given by the function $E_{\text{cut}} = (20.17 \pm 0.06) + (0.30 \pm 0.06) \times (\text{ASM} - 5.0)$ (all values in keV). Pearson's linear correlation coefficient is 0.74.

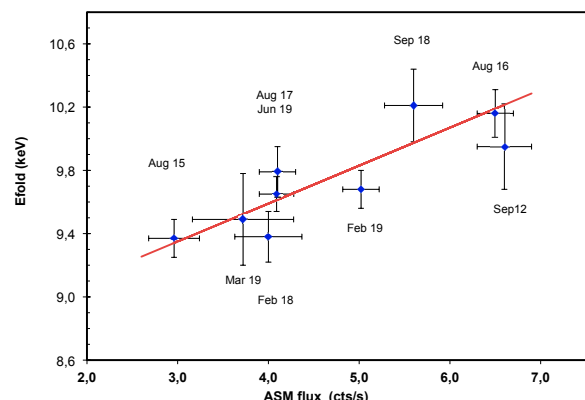


Fig. 8. The continuum parameter E_{fold} versus X-ray flux in units of (ASM-cts/s). The best fit line is given by the function $E_{\text{fold}} = (9.83 \pm 0.04) + (0.24 \pm 0.03) \times ((\text{ASM} - \text{cts/s}) - 5.0)$ (all values in keV). Pearson's linear correlation coefficient is 0.79.

In addition, we give the linear correlation between the relative line width σ / E_{cyc} to the optical depth τ (Fig.6), a correlation first noticed by Coburn et al. (2002) in a group of cyclotron line objects. As with other correlations, also this one can be realized in individual objects - here Her X-1, also in 4U 1538–52 (Rodes-Roca et al. 2008). This may not be so easy to understand in the context of theoretical considerations (see discussion).

3.2. Continuum parameters

The systematic monitoring of Her X-1 with *NuSTAR* over the last decade has allowed the discovery that all continuum param-

eters, E_{cut} , E_{fold} and Γ are systematically correlated with X-ray flux. The correlations can be described by linear functions, see Table 4, Fig. 7, Fig. 8 and Fig. 9. Since both E_{cut} and E_{fold} depend on X-ray flux, they correlate with each other which is shown in Fig. 10. Normalizing E_{cut} and E_{fold} to the reference flux of 5.0 (ASM-cts/s), we find that both normalized parameters (excluding the values of cycle 494/Feb 2019, where the 35d-phase is very high, see Sect. 3.4) are consistent with a constant value over the time span 2012–2019 (Fig. 13). In calculating the dependence of Γ on flux we have excluded the exceptionally low value (0.885) measured in February 2019 (cycle 494, see Table 2) because the observation happened at a high 35-day phase of 0.202, where the flux is about 65% of the maximum *Main-On*

Table 4. The linear dependence of spectral parameters on X-ray flux. The five line parameters are the centroid energy E_{cyc} , the width σ_{cyc} , the line "strength", the optical depth τ (see eq. 2) and the relative width $\sigma_{\text{cyc}}/E_{\text{cyc}}$. The three continuum parameters are E_{cut} and E_{fold} and the power law photon index Γ . The X-ray flux is measured in units of (ASM-cts/s), referring to the All Sky Monitor of *RXTE*: $y = a + b(x - c)$. Here, the offset in x is always constant: $c = 5.0$ (ASM-cts/s) (close to the center of the range of fluxes observed). We note that 5.0 (ASM-cts/s) corresponds to $5.0 \times 0.237 = 1.18$ (keV/cm² s) in (2–10 keV). Uncertainties are at the 1 sigma (68%) level. The last column lists Pearson's linear correlation coefficients.

Parameters	a [keV] or no dimension	b^d	Pearson's corr. coeff.
E_{cyc}^a [keV]	36.24 ± 0.09	0.675 ± 0.075	0.98
σ_{cyc}^b [keV]	5.30 ± 0.09	0.41 ± 0.07	0.99
strength ^c	7.28 ± 0.22	1.15 ± 0.19	0.96
opt. depth τ^c	0.54 ± 0.02	0.042 ± 0.015	0.87
$\sigma_{\text{cyc}}/E_{\text{cyc}}$	0.146 ± 0.002	0.0086 ± 0.0002	0.97
E_{cut} [keV]	20.17 ± 0.06	0.30 ± 0.06	0.74
E_{fold} [keV]	9.83 ± 0.04	0.24 ± 0.03	0.79
Γ	0.965 ± 0.002	0.015 ± 0.001	0.53

^a Fig. 1; ^b Fig. 3; ^c we note that strength [keV] = $\sigma \times \tau \times \sqrt{2\pi}$;
^d [keV/(ASM-cts/s)] or [1/(ASM-cts/s)]

flux of this cycle. At 35-day phases beyond ~ 0.16 , Γ is known to decrease (Vasco 2012). The measured increase of Γ on flux is fairly weak but interesting because this is in disagreement with reports about a correlation in the opposite sense by Klochkov et al. (2011) (see the discussion below).

3.3. Correlation between line and continuum parameters

Since the continuum parameters E_{cut} and E_{fold} and all cyclotron line parameters correlate with X-ray flux, there are correlations between the line and the continuum parameters. As two examples we list the linear correlation parameters of the observed cyclotron line energy and the continuum parameters in Table 3 and show them in Fig. 11 and Fig. 12.

3.4. Dependence on phase of the 35-day modulation

As mentioned in the Introduction, Her X-1 shows a regular 35-day modulation, known since the discovery of the source by *UHURU* (Tananbaum et al. 1972), thought to be connected with the precession of the accretion disk providing regular shadowing of the X-ray source. The 35-day periodicity is also seen in the regular variations of the shape of the pulse profiles (Trümper et al. 1986; Staubert et al. 2013), which has also led to the suggestion that free precession of the neutron star may play a role (Trümper et al. 1986; Postnov et al. 2013), which is still an open question and highly debated. In the context of this work it is of interest whether the X-ray spectra show variations with phase of the 35-day modulation. This is indeed the case (Parmar et al. 1980; Mihara et al. 1991; Kuster et al. 2005; Vasco 2012). Staubert et al. 2014 had suggested that there is a weak modulation of the cyclotron line energy E_{cyc} during the *Main-On* and Vasco 2012 had found a strong variation of the power law index for 35-day phases greater than 0.16. The contribution of the series of *NuSTAR* observations of Her X-1, discussed here, is the following (for the limited range provided by the data used here, see Table 1): 1) The flux normalized E_{cyc} does not show any

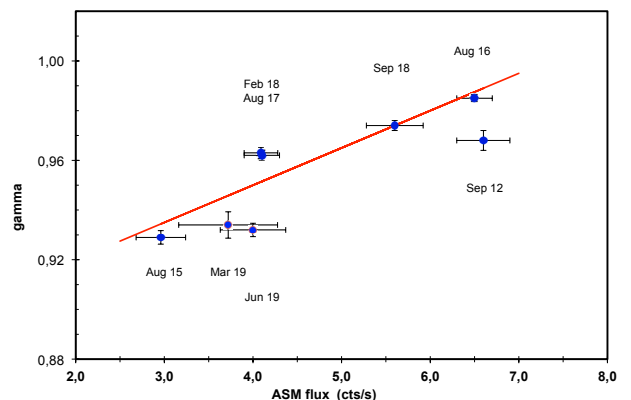


Fig. 9. The power law index Γ versus flux in (ASM-cts/s). The best fit line is given by the function $\Gamma = (0.965 \pm 0.002) + (0.015 \pm 0.001) \times ((\text{ASM-cts/s}) - 5.0)$. This function is valid for 35-day phases up to 0.16. The low Γ value measured in Feb 2019 (cycle 494, see Table 2) was not included in this fit because the observation took place at a 35-day phase of 0.202, at which a lower value is expected (see text). Pearson's linear correlation coefficient is 0.53.

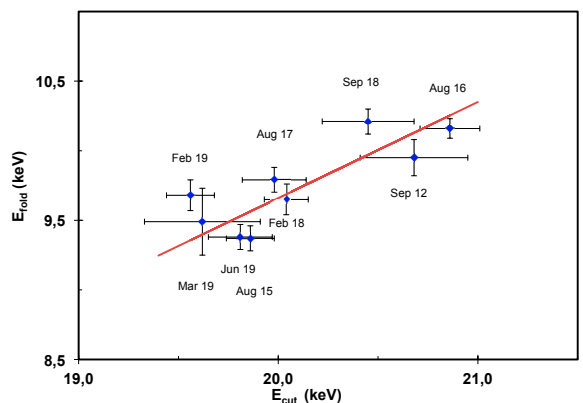


Fig. 10. The continuum parameter E_{fold} versus the continuum parameter E_{cut} . The best fit line is given by the function $E_{\text{fold}} = (9.66 \pm 0.05) + (0.69 \pm 0.12) \times (E_{\text{cut}} - 20.0)$ (all values in keV). Pearson's linear correlation coefficient is 0.82.

variation, the values are consistent with a constant. 2) The flux normalized values of E_{cut} and E_{fold} are constant up to the second highest 35-day phase observed (0.147 for Aug 2017, cycle 478), then both drop to significant lower values for the highest observed 35-day phase (0.202 for Feb 2019, cycle 494). 3) The normalized power law index Γ behaves as the other two continuum parameters and drops to the lowest value (0.885) for the Feb 2019 observation at 35-day phase 0.202.

4. Discussion

Correlations between spectral parameters were first discovered by comparing spectral parameters determined for different objects (Makishima & Mihara 1992; Makishima et al. 1999; Coburn et al. 2002). We now see, most prominently (but not only) in Her X-1, that strong correlations between spectral pa-

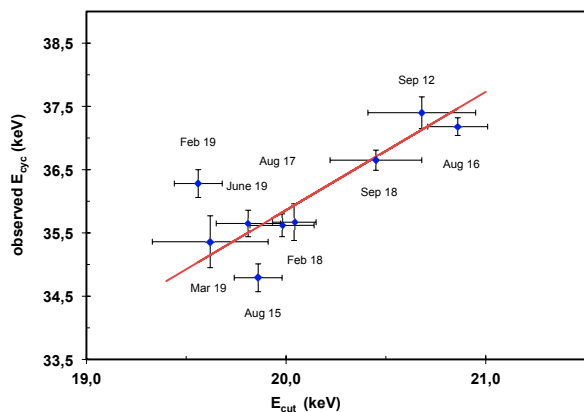


Fig. 11. The observed cyclotron line energy versus E_{cut} . The best fit line is given by the function $E_{\text{cyc}} = (35.86 \pm 0.11) + (1.87 \pm 0.36) \times (E_{\text{cut}} - 20.0)$ (all values in keV). Pearson's linear correlation coefficient is 0.79.

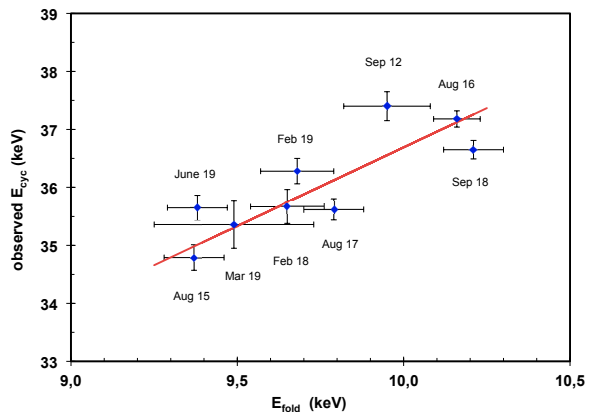


Fig. 12. The observed cyclotron line energy versus E_{fold} . The best fit line is given by the function $E_{\text{cyc}} = (36.69 \pm 0.13) + (2.71 \pm 0.39) \times (E_{\text{fold}} - 10.0)$ (all values in keV). Pearson's linear correlation coefficient is 0.82.

rameters, both continuum and line parameters, exist for individual objects, particularly related to changes in X-ray luminosity.

4.1. Correlation between line parameters

The linear correlation between the width of the cyclotron line and its centroid energy (Fig. 4) is expected from the fact that the line suffers a Doppler-broadening due to the thermal motion of the electron gas at a temperature kT_e . Applying the general formula for a Doppler-broadened line (of central energy E) to the resonant cyclotron scattering of photons on electrons, we write $\sigma = E (kT_e / m_e c^2)^{1/2}$.¹¹ Because electrons in a strong magnetic field can move freely only in one dimension (along the field lines) we need to multiply by $\cos \theta$, with θ being the angle between the viewing direction and the magnetic field lines. The temperature of the electron gas is kT_e and the rest mass of the electron is $m_e c^2 \approx 511$ keV, so the electron temperature can be estimated to $kT_e [\text{keV}] \approx 511 (\sigma / E_{\text{cyc}})^2 / |\cos^2 \Theta|$. The line broadening effect was already pointed out by Trümper et al. (1977) when the discovery of the first cyclotron line - in Her X-1 - was reported (see also Meszaros & Nagel 1985; Orlandini et al. 1998). It was then observationally confirmed when different cyclotron line energies and associated widths in several X-ray binaries were measured (Makishima et al. 1999; Coburn et al. 2002). Recently, it became possible to observe such correlations in individual sources, when the CRSF energy as well as the line width change with varying flux. Here we report the measurement for Her X-1: $\sigma = 5.26 + 0.60 (E_{\text{cyc}} - 36.0)$ (all in keV). For small θ ($\cos \theta \sim 1$), the calculated kT_e ranges from 8.3 keV to 13.5 keV, for flux values from 3 to 7 ASM-cts/s, respectively. This is very close to 10 keV which is the typical value of the continuum parameter E_{fold} , often taken as the temperature of the plasma emitting the continuum. It is tempting to conclude that in Her X-1 we most likely see a pencil beam rather than a fan beam.

The fact that the relative line width σ / E_{cyc} increases with increasing flux (Fig. 5) means that the electron temperature kT_e increases with increasing flux. And so does E_{fold} , as expected

¹¹ The general formula for a Doppler-broadened line is $\text{FWHM} = E \times (8 \ln 2 kT_e / m_e c^2)^{1/2}$, with E being the line energy and $\text{FWHM} = \sigma (8 \ln 2)^{1/2} = 2.356 \sigma$ being the full width-at-half-maximum (see, e.g., K.R. Lang, *Astrophysical Formulae*, Springer).

for an increasing accretion rate. However, the magnitude of the increase in kT_e is $\sim 12\%$ per unit flux, significantly stronger than the increase in E_{fold} with only $\sim 2\%$. If E_{fold} is indeed a measure of the continuum temperature, then the electron temperature is increasing significantly faster.

The general dependence of σ on E_{cyc} for the known cyclotron line objects is demonstrated in Fig. 14 (up to $E_{\text{cyc}} = 60$ keV), where pairs of σ and E_{cyc} values are shown, taken from Coburn et al. (2002) and Staubert et al. (2019) (their Table A.5), together with a few individual objects. The central line through the rather scattered data defines a slope of ~ 0.18 keV/keV, corresponding to a mean kT_e of ~ 16 keV for $\Theta = 0$. For a few objects we have now observed variations of both the line energy and the line width (physically introduced by a changing X-ray flux): Her X-1 (Staubert et al. 2007 and this work), GX 304-1 (Klochkov et al. 2015; Malacaria et al. 2015; Rothschild et al. 2017), Vela X-1 (La Parola et al. 2016) (the first harmonic) and Swift J1626.6-5156 (DeCesar et al. 2013) (see Fig. 14). For these few objects the absolute values of the relative widths are all rather small (they are all below the red line in Fig. 14, but the variation $d(\sigma) / d(E_{\text{cyc}})$, is significantly steeper (e.g., for Her X-1: 0.60 keV/keV), than for the complete ensemble.

We would like to stress that the X-ray flux (physically the mass accretion rate) is a fundamental parameter that seems to influence all spectral parameters. Apart from the line position and width, also its strength, its depth and its relative width are positively correlated with flux (see Table 4). The same is true for the continuum parameters E_{cut} and E_{fold} (Fig. 7 and Fig. 8), and - surprisingly (even if weak) - for the power law index Γ . We find that Γ increases with flux (by 1.8% for an increase in flux by a factor of two), while Klochkov et al. (2011), in pulse-amplitude-resolved spectroscopy of Her X-1, found the opposite trend (by 5.6%) - always in combination with an increase of E_{cyc} with flux. A solution may be given by Postnov et al. (2015) who showed (for several sources, but unfortunately not Her X-1) that the spectral hardness correlates with X-ray flux, consistent with Klochkov et al. (2011), but only up to a (source dependent) luminosity around a few times 10^{37} erg/s, after which the correlation stops, or even reverses. A luminosity of a few times 10^{37} erg/s is considered to be close to the border between the sub- and super-critical accretion regimes (Becker et al. 2012) at which the trend

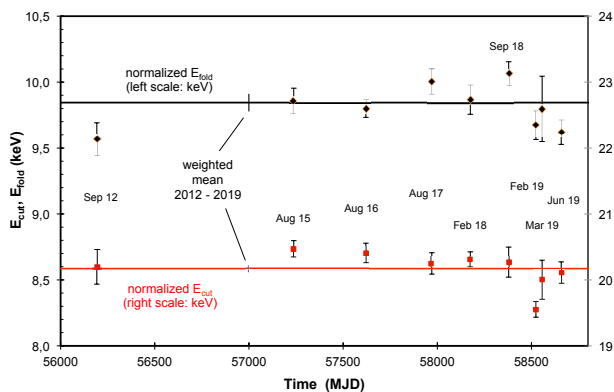


Fig. 13. Flux normalized values of E_{cut} (right scale) and E_{fold} (left scale) as function of time. The normalization to a reference X-ray flux of 5 (ASM-cts/s) uses the linear correlations as stated in Table 4 and shown in Figs. 7 and 8. These two continuum parameters appear to be constant (see the horizontal lines) over the time 2012–2019, except for Feb 2019 where the 35d-phase is very high (0.202).

for these correlations reverses. Her X-1 is probably operating close to the critical luminosity, and the turning point for a reversal may actually be slightly different between the respective correlations.

An interesting correlation, first found by Coburn et al. (2002) among a group of X-ray binaries, namely the relative line width $\sigma_{\text{cyc}} / E_{\text{cyc}}$ as function of the optical depth τ , is also realized in individual objects like 4U 1538–52 (Rodes-Roca et al. 2008) and in Her X-1 (Fig. 6). Coburn et al. (2002) and Rodes-Roca et al. (2008) note that simple theoretical models of cyclotron line generation actually predict the opposite dependence (Isenberg et al. 1998; Araya & Harding 1999).

Regarding inter-correlations between spectral parameters, it has been a general worry about how large the influence is of purely mathematical correlations introduced in the fitting process. Coburn et al. (2002) have tried to answer this question by performing Monte Carlo simulations, carefully designed for different types of correlations. Their conclusion was that formal correlations were not significant and that it was safe to conclude that the observed correlations are a true physical effect. We have used the Markov Chain Monte Carlo (MCMC) procedure offered in XSPEC to investigate the same question and present a corresponding analysis in Appendix A. We are confident that the observed correlations are indeed physical.

4.2. Physics behind changes of E_{cyc}

The centroid energy of the cyclotron line in Her X-1 has been observed to change with respect to the following parameters (Staubert et al. 2014):

- pulse phase: 20% ((max-min)/mean) (Voges et al. 1982; Vasco et al. 2013; Staubert et al. 2014);
- X-ray flux: 6.5% for a change of flux by a factor of two (here and Staubert et al. 2007);
- elapsed time: constant around 35 keV from the discovery in 1975 to 1990, jump upward 1991–1994 from ~ 35 keV to beyond 40 keV ($\sim 20\%$) (Gruber et al. 2001; Staubert et al. 2007), followed by a well measured decay until ~ 2012 down to ~ 37 keV (10% over 16 years) (here and Staubert et al. 2014, 2016);
- and possibly a change by 1 keV or less with phase of the 35-

day on-off-cycle (Staubert et al. 2014), which we do not confirm here.

The variation with pulse phase is believed to be due to the changing viewing angle under which the emission regions are seen (Schönherr et al. 2007). Vasco 2012¹² has shown that the above discussed correlation between the width and the centroid energy of the cyclotron line (and the dependence of both on flux) is also valid when certain pulse phases are analyzed (e.g., the line energy and the width are both at a maximum around the peak of the main pulse). We will not further discuss this phenomenon here, but concentrate on the dependence of the pulse phase averaged cyclotron line energy E_{cyc} on X-ray flux and on time.

4.2.1. Changes of E_{cyc} with flux

With respect to the physics at work behind the positive correlation of the pulse phase averaged cyclotron line energy with flux, we refer to discussions presented earlier by Staubert et al. (2007, 2014, 2016, 2017); Ji et al. (2019), as well as the theoretical work by Becker et al. (2012) (see also the summary and references given in the review by Staubert et al. (2019)). Here detailed modeling of the physics is necessary: what is the mechanism of deceleration of the accreted material? Is it due to simple Coulomb scattering or the generation of radiative shocks? What kind of accretion rate is necessary to generate such shocks and at which height above the neutron star surface would they form? What is the configuration of the magnetic field, most likely influenced by the in-falling material? It has become popular to talk about ‘accretion regimes’ (e.g., Becker et al. 2012): ‘sub-critical’ and ‘super-critical’ accretion, most likely separated by a critical luminosity of the order of a few times 10^{37} erg/s. Generally, the ‘sub-critical’ accretion is associated with a positive E_{cyc}/L_x correlation, and the ‘super-critical’ accretion with a negative correlation (Becker et al. 2012; Mushtukov et al. 2015). Recently, a model involving a collisionless shock was developed that also explains the deviation from a pure linear dependence (a ‘roll-off’), as observed in GX 304–1 (Rothschild et al. 2017; Vybornov et al. 2017). A more detailed discussion is presented in Staubert et al. (2017).

Alternatively, or in combination with a height-related effect, the observed variations could be due to changes of the configuration of the magnetic field when the accretion rate varies. As Mukherjee et al. (2013, 2014) have shown, the usually assumed dipole structure of the magnetic field is significantly altered when the mass accretion rate changes. Close to the magnetic poles, a higher accretion rate can lead to a significant increase of the density of field lines at the outer circumference of the accretion mound when the in-falling material pushes matter and field lines from the center radially outward. See also the Discussion in Bala et al. (2020).

4.2.2. Changes of E_{cyc} with time

The dependence of E_{cyc} on time is even less well understood. With regard to the long-term decay of E_{cyc} , we think that it is either a geometric displacement of the emission region or a change in the local field configuration e.g., as calculated by Mukherjee & Bhattacharya (2012), rather than a change in the strength of the underlying global dipole. Staubert (2014) has suggested that the observed change of E_{cyc} may be connected to a slight imbalance between ‘gain’ and ‘loss’ of accreted material, such that

¹² PhD thesis by Davide Vasco, 2012, University of Tübingen, Germany, <http://nbn-resolving.de/urn:nbn:de:bsz:21-opus-63466>

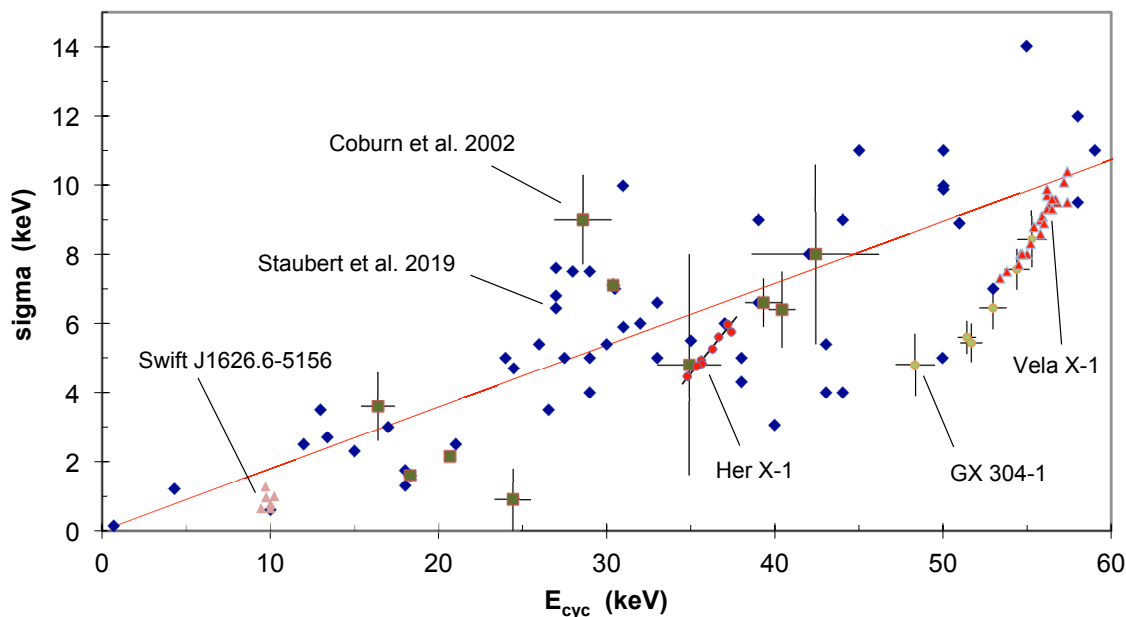


Fig. 14. Correlation between the width (σ) and the centroid energy of cyclotron lines for different X-ray binaries. The blue rhombs are data from the compilation in Staubert et al. (2019), the filled squares (with uncertainties) are from Coburn et al. (2002). The red line is a fit to these two data sets defining $\sigma = 0.18 E_{\text{cyc}}$. The individual sources shown are: GX 304-1 (Klochkov et al. 2015), Swift J1626.6-5156 (DeCesar et al. 2013), Vela X-1 (La Parola et al. 2016) and Her X-1 (same as Fig. 4).

the structure of the accretion mound changes with time. With an accretion rate of $\sim 10^{17}$ g/s a variation on relatively short time scales does not seem implausible. If the “gain” is slightly larger than the “loss”, material would slowly accumulate in the mound, possibly increasing its height or changing the local field structure, which might be the reason for the long-term reduction in E_{cyc} . One might expect, that this reduction can find a natural end (e.g., when the excess mass and the associated pressure in the accretion mound becomes too large), such that a forced outflow of material to larger areas of the NS surface causes a re-adjustment of the accretion mound back to the un-perturbed configuration. This could be a relatively fast and catastrophic event – possibly explaining the rather sudden upward jump in E_{cyc} observed between 1990 and 1993. The time period 1990-2012 sets an apparent time scale of instability: a few years of very fast change – the increase in E_{cyc} by ~ 5 keV –, followed by ~ 16 years of decay down to the original level. A corresponding time scale for stability is not yet known. Future observations should search for indications for an increase or even a new upward jump in E_{cyc} . Since an upward movement could be rather fast (similar to the earlier event), it is important to observe as regularly as possible, in order not to miss such an event again.

5. Summary

Her X-1 has been well monitored during the last decade, mostly by *NuSTAR*, but also by *INTEGRAL* and *Swift/BAT*, and more recently by *Insight-HXMT* (Xiao et al. 2019) and *Astrosat* (Bala et al. 2020). Her X-1 is the only highly magnetized accreting

pulsar for which repeated observations over longer periods of time exist. This has provided the base for the discovery of new phenomena, like the dependence of the cyclotron line energy (as well as almost all spectral parameters) on flux and the long-term decay of the cyclotron line energy over nearly 20 years. Both of these phenomena have meanwhile been seen in other accreting X-ray binary pulsars (see the review by Staubert et al. 2019).

The results of nine *NuSTAR* observations of Her X-1 between 2012 and 2019 are the following:

- The dependence of the cyclotron line energy on X-ray flux, discovered in 2007, is confirmed and measured with high precision.
- The flux-normalized cyclotron line energy is constant since (at least) ~ 2012 . The previously reported long-term decay has ended.
- All cyclotron line parameters - the line energy E_{cyc} , the width σ , the strength, the optical depth τ and the relative width - show a positive and linear correlation to X-ray flux.
- The former statement also means that all cyclotron line parameters correlate positively and linearly with one-another.
- The continuum parameters E_{cut} and E_{fold} correlate positively and linearly with X-ray flux. The flux-normalized continuum parameters are consistent with constant values since 2012. The third continuum parameter, the power law index Γ , shows a weak positive correlation with flux. This is the opposite of what was seen before in a pulse-amplitude-resolved analysis, which may have a somewhat different meaning. The interpretation of the different observed correlations with regard to the prevailing accretion regimes (sub- or supercritical) is not so simple.
- We have learned that there are correlations between continuum

parameters and line parameters.

- The correlations of the line and continuum parameters with X-ray flux and among each other are considered to reflect true physical correlations, which have yet to be investigated and explained by theoretical modeling. As shown in the Appendix, the analysis of the purely mathematical correlation between fitting parameters has led to the conclusion that those are not significant.

We urge that the source continues to be observed regularly. For 2020 this seems to be secured through already planned observations (partly simultaneous) between *INTEGRAL*, *NuSTAR*, *XMM-Newton* and *Insight-HXMT*. At the same time, it would be very important that theoretical models be developed further.

Acknowledgements. We would like to acknowledge the dedication of all the people who have contributed to the great success of all relevant missions, in particular *NuSTAR*. We especially thank the “schedulers”, foremost Karl Forster, for his efforts with respect to the non-standard scheduling of the observations of Her X-1. We acknowledge the historical contributions to the subject at hand by Dmitry Klochkov. We thank the anonymous referee for valuable comments.

References

- Araya, R. & Harding, A. 1999, *ApJ*, 517, 334
- Bala, S., Bhattacharya, D., Staubert, R., & Maitra, C. 2020, *MNRAS*, 497, 1029
- Becker, P. A., Klochkov, D., Schönherr, G., et al. 2012, *A&A*, 544, A123
- Caballero, I. & Wilms, J. 2012, *Mem. Soc. Astron. Italiana*, 83, 230
- Coburn, W., Heindl, W. A., Rothschild, R. E., et al. 2002, *ApJ*, 580, 394
- DeCesar, M. E., Boyd, P. T., Pottschmidt, K., et al. 2013, *ApJ*, 762, 61
- Foreman-Mackey, D., Hogg, D. W., Lang, D., & Goodman, J. 2013, *PASP*, 125, 306
- Fürst, F., Grefenstette, B. W., Staubert, R., et al. 2013, *ApJ*, 779, 69
- Gerend, D. & Boynton, P. E. 1976, *ApJ*, 209, 562
- Gruber, D. E., Heindl, W. A., Rothschild, R. E., et al. 2001, *ApJ*, 562, 499
- Harrison, F. A., Craig, W. W., Christensen, F. E., et al. 2013, *ApJ*, 770, 103
- Heindl, W. A., Rothschild, R. E., Coburn, W., et al. 2004, in *American Institute of Physics Conference Series*, Vol. 714, *X-ray Timing 2003: Rossi and Beyond*, ed. P. Kaaret, F. K. Lamb, & J. H. Swank, 323–330
- Isenberg, M., Lamb, D. Q., & Wang, J. C. L. 1998, *ApJ*, 493, 154
- Ji, L., Staubert, R., Ducci, L., et al. 2019, *MNRAS*, 484, 3797
- Klochkov, D., Staubert, R., Postnov, K., et al. 2008, *A&A*, 482, 907
- Klochkov, D., Staubert, R., Postnov, K., et al. 2015, *A&A*, 578, A88
- Klochkov, D., Staubert, R., Santangelo, A., Rothschild, R. E., & Ferrigno, C. 2011, *A&A*, 532, A126
- Klochkov, D. K., Shakura, N. I., Postnov, K. A., et al. 2006, *Astronomy Letters*, 32, 804
- Kuster, M., Wilms, J., Staubert, R., et al. 2005, *A&A*, 443, 753
- La Parola, V., Cusumano, G., Segreto, A., & D’Ai, A. 2016, *MNRAS*, 463, 185
- Makishima, K. & Mihara, T. 1992, *Frontiers O X-ray Astronomy* (Universal Academy Press Inc, Tokyo), 23
- Makishima, K., Mihara, T., Nagase, F., & Tanaka, Y. 1999, *ApJ*, 525, 978
- Malacaria, C., Klochkov, D., Santangelo, A., & Staubert, R. 2015, *A&A*, 581, A121
- Meszáros, P. & Nagel, W. 1985, *ApJ*, 298, 147
- Mihara, T., Ohashi, T., Makishima, K., et al. 1991, *PASJ*, 43, 501
- Mukherjee, D. & Bhattacharya, D. 2012, *MNRAS*, 420, 720
- Mukherjee, D., Bhattacharya, D., & Mignone, A. 2013, *MNRAS*, 435, 718
- Mukherjee, D., Bhattacharya, D., & Mignone, A. 2014, in *European Physical Journal Web of Conferences*, Vol. 64, *European Physical Journal Web of Conferences*, 2004
- Mushtukov, A. A., Suleimanov, V. F., Tsygankov, S. S., & Poutanen, J. 2015, *MNRAS*, 447, 1847
- Orlandini, M., Dal Fiume, D., Frontera, F., et al. 1998, *ApJ*, 500, L163
- Parmar, A. N., Sanford, P. W., & Fabian, A. C. 1980, *MNRAS*, 192, 311
- Petterson, J. A. 1977, *ApJ*, 218, 783
- Postnov, K., Shakura, N., Staubert, R., et al. 2013, *MNRAS*, 435, 1147
- Postnov, K. A., Gornostaev, M. I., Klochkov, D., et al. 2015, *MNRAS*, 452, 1601
- Revnivtsev, M. & Mereghetti, S. 2016, *Magnetic Fields of Neutron Stars in X-Ray Binaries*, Vol. 54 (Springer 2016), 299
- Reynolds, A. P., Quaintrell, H., Still, M. D., et al. 1997, *MNRAS*, 288, 43
- Rodes-Roca, J., Torrejón, J. M., & Bernabéu, J. G. 2008, *The fundamental cyclotron line in 4U 1538-52*, Vol. 3, 189–200
- Rothschild, R. E., Kühnel, M., Pottschmidt, K., et al. 2017, *MNRAS*, 466, 2752
- Sazonov, S., Paizis, A., Bazzano, A., et al. 2020, arXiv e-prints, arXiv:2006.05063
- Schandl, S. & Meyer, F. 1994, *A&A*, 289, 149
- Schönherr, G., Wilms, J., Kretschmar, P., et al. 2007, *A&A*, 472, 353
- Schwarm, F.-W., Schönherr, G., Falkner, S., et al. 2017, *A&A*, 597, A3
- Staubert, R. 2003, in *Multifrequency behaviour of high energy cosmic sources*, ed. L.S.-G.F. Giovannelli, Vol. ChJAA, Vol. 3, S270
- Staubert, R. 2014, in *PoS(INTEGRAL2014)024*
- Staubert, R., Bezler, M., & Kendziorra, E. 1983, *A&A*, 117, 215
- Staubert, R., Klochkov, D., Fürst, F., et al. 2017, *A&A*, 606, L13
- Staubert, R., Klochkov, D., Vasco, D., et al. 2013, *A&A*, 550, A110
- Staubert, R., Klochkov, D., Vyborno, V., Wilms, J., & Harrison, F. A. 2016, *A&A*, 590, A91
- Staubert, R., Klochkov, D., Wilms, J., et al. 2014, *A&A*, 572, A119
- Staubert, R., Shakura, N. I., Postnov, K., et al. 2007, *A&A*, 465, L25
- Staubert, R., Trümper, J., Kendziorra, E., et al. 2019, *A&A*, 622, A61
- Tananbaum, H., Gursky, H., Kellogg, E. M., et al. 1972, *ApJ*, 174, L143
- Terada, Y., Mihara, T., Nagase, F., et al. 2007, *Adv. in Space Research*, 40, 1485
- Trümper, J., Kahabka, P., Oegelman, H., Pietsch, W., & Voges, W. 1986, *ApJ*, 300, L63
- Trümper, J., Pietsch, W., Reppin, C., et al. 1978, *ApJ*, 219, L105
- Trümper, J. et al. 1977, *Ann. N.Y. Acad. Sci.*, 302, 538
- Vasco, D. 2012, PhD thesis, Univ. of Tübingen
- Vasco, D., Staubert, R., Klochkov, D., et al. 2013, *A&A*, 550, A111
- Voges, W., Pietsch, W., Reppin, C., et al. 1982, *ApJ*, 263, 803
- Vyborno, V., Klochkov, D., Gornostaev, M., et al. 2017, *A&A*, 601, A126
- Wilms, J. 2012, in *Proceed. 39th COSPAR Sci. Assembly*, 14-22 July 2012, Mysore, India, Vol. 39, 2159
- Wolff, M. T., Becker, P. A., Gottlieb, A. M., et al. 2016, *ApJ*, 831, 194
- Xiao, G. C., Ji, L., Staubert, R., et al. 2019, *Journal of High Energy Astrophysics*, 23, 29

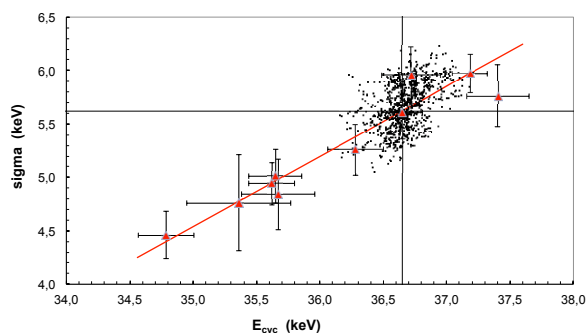


Fig. A.1. The first 1000 σ / E_{cyc} pairs of the MCMC simulation together with the measured correlation as shown in Fig. 4.

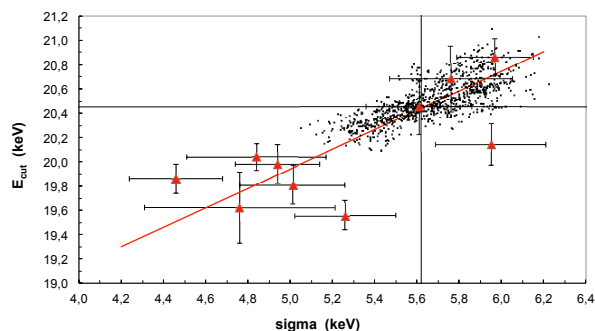


Fig. A.2. The first 1000 E_{cut} / σ pairs of the MCMC simulation together with the measured correlation.

Appendix A: Appendix

In the main text, we reported the correlations between spectral parameters observed from nine *NuSTAR* observations in 2012-2019. Here we ask how much model degeneracies during the spectral fitting contribute to these correlations. We investigate this through Monte Carlo simulations. In practice, we adopted the best-fitting parameters of the *NuSTAR* observation in September 2018 as a reference model (with a flux of 5.6 (ASM-cts/s) this observation is close to the center of the flux range encountered between 2012 and 2019). With the statistics and the spectral parameters from this observation as an input model, we performed two different simulations (with 10^4 events each): first, a Markov Chain Monte Carlo (MCMC) simulation (provided by XSPEC¹³) which makes use of the Goodman-Weare algorithm¹⁴ (see also Foreman-Mackey et al. (2013)), and second producing simulated spectra using the *fakeit* command in XSPEC with subsequently fitting these spectra. The two methods provided consistent results, we show the MCMC simulation in Fig. A.3.

As expected, most of the correlations between the parameters are weak, as is evident from the circular shape of the two-dimensional distributions. As an example we show the scatter

plot of σ_{cyc} versus E_{cyc} of the first 1000 simulated MCMC spectra in Fig. A.1. The range of observed E_{cyc} is a factor ~ 10 larger than the corresponding full width at half maximum (FWHM) of the simulated E_{cyc} distribution (for σ_{cyc} the factor is ~ 3.3). This shows that any model degeneracy has only a minor contribution to the overall correlation. There are three distributions that are elongated (under roughly 45 degrees) indicating stronger correlations: D_{cyc}^{15} versus σ_{cyc} , E_{cut} versus σ_{cyc} and E_{cut} versus D_{cyc} . Even here the corresponding factors (FWHM / observed range) are between two and four. The correlation between σ_{cyc} and D_{cyc} is actually given through the definition: $D_{\text{cyc}} = \sigma \times \tau \times \sqrt{2\pi}$. In Fig. A.2 we show the degeneracy between the continuum parameter E_{cut} and the line parameter σ_{cyc} . We conclude that the physical correlations discussed are real.

¹³ <https://heasarc.gsfc.nasa.gov/xanadu/xspec/>

¹⁴ <https://ui.adsabs.harvard.edu/abs/2010CAMCS...5...65G/abstract>

¹⁵ D_{cyc} is called *strength* in the main text

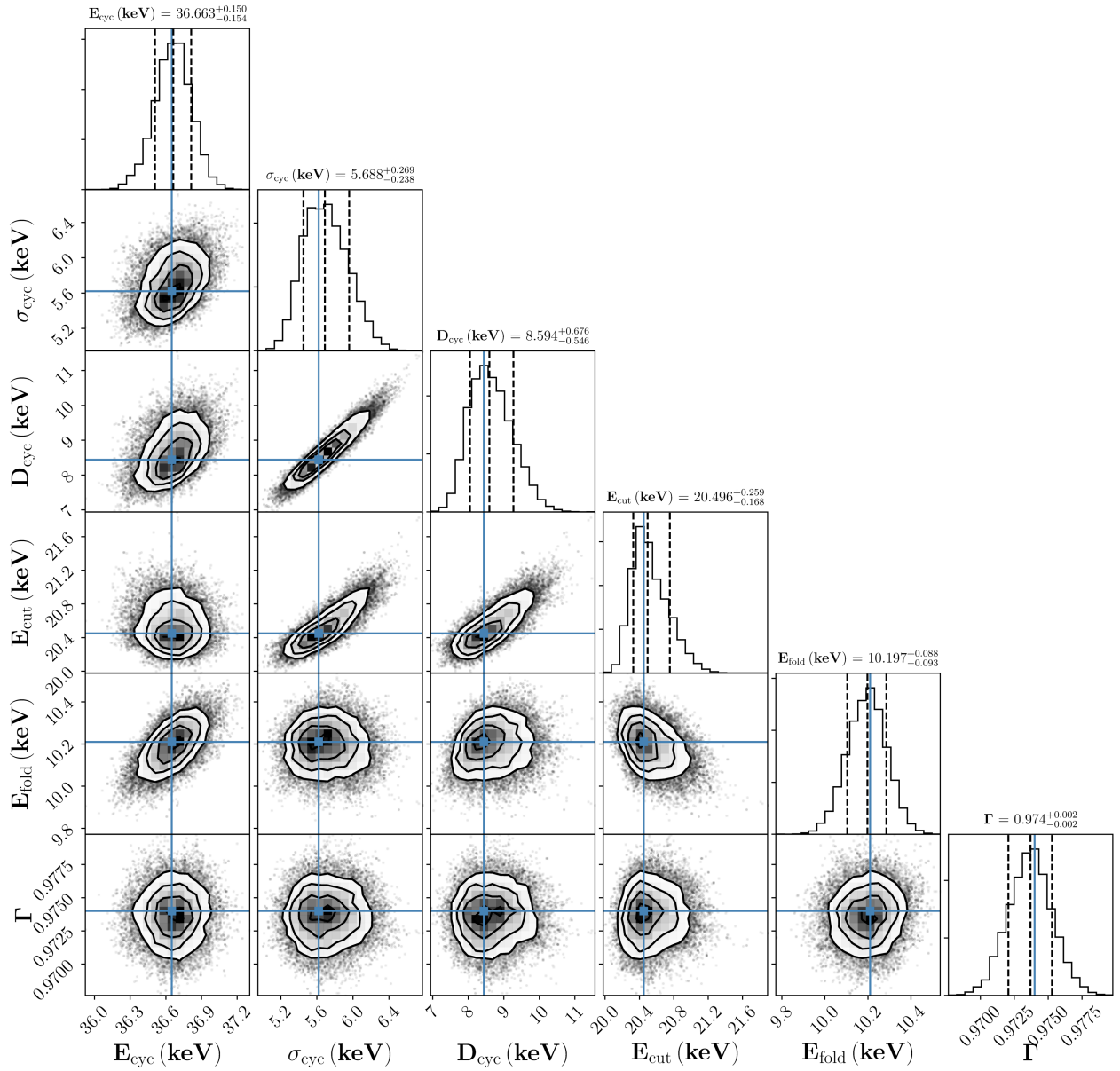


Fig. A.3. The contours represent two-dimensional distributions of parameters obtained from Monte Carlo simulations at the significance level of 1, 2 and 3 σ , and the histograms are distributions for each variable. The blue lines are the input parameters used during the simulations.